ACTUATORS

# Electrofluidic fiber muscles

O. K. Afsar[1]*, G. Pupillo[1,2], G. Vitucci[2], W. Babatain[1], H. Ishii[1], V. Cacucciolo[1,2]*



**Actuators are to robots what muscles are to humans. They enable motion and determine strength and dexterity. The fiber form factor makes skeletal muscles modular, scalable, and densely integrated (50% of human body weight). In contrast, servo motors that drive today's robots lack the flexibility and modularity of muscle fibers, limiting integration and dexterity. Here, we report electrofluidic fiber muscles, soft artificial muscles for robotic applications with power density comparable to skeletal muscles (50 watts per kilogram), contraction strains of 20%, and response time of 0.3 second. These 2-millimeter-thick muscles comprise antagonistic fluidic actuators driven by electrohydrodynamic fiber pumps in a closed circuit. They require no external liquid reservoir and are electrically driven, untethered, and silent. We demonstrated that performance is increased by pre-pressurizing the muscles at an optimal bias pressure. Applying bias pressure allowed the antagonist actuator to act as a reservoir for the agonist, enabled 200% higher operating voltages by preventing cavitation, and leveraged the nonlinear pressure-stroke response of the actuators, increasing strain threefold at a given pump pressure. We characterized and modeled their dynamics, identifying optimal bias pressures. Electrofluidic muscles scale by simply bundling fibers. By selecting the ratio between pumps and actuators, we programmed their performance for different robotic tasks: a fast lever (180 millimeters per second) that launches objects in <0.3 second; a strong bundle that lifts 4 kilograms (200 times its weight) with a 30-millimeter stroke; a woven muscle that bends a robot arm by 40° and is compliant enough for a human handshake.**

## INTRODUCTION

Nearly all animal muscles are organized as bundles of fibers, whereas nearly all robots are driven by electromagnetic (EM) servo motors, which have bulky cylindrical shapes. EM motors offer high power density and are efficient and reliable, yet their form factor limits integration in robots with soft body parts (*1*) and in wearable robots (*2*). Transmitting motion to anything other than rotary joints requires additional components such as pulleys and tendons. On the contrary, biological muscle fibers can be modularly organized into structures, with force easily scaled by increasing the number of fibers in each bundle.

To overcome the limitations of EM motors, researchers have developed fluidically and electrically driven soft actuators. These actuators are easy to manufacture, robust, and scalable, and they have been used in soft grippers (*3*–*6*), walking robots (*7*, *8*), swimming robots (*9*–*11*), wearables (*12*, *13*), and even large-scale deployable robots (*14*). The main limitation of fluidic actuators is the bulky pneumatic infrastructure required to operate them, which has so far hindered their adoption in commercial robots, except for industrial grippers. Conversely, electrically driven actuators have the advantage of directly converting electrical energy from a battery into mechanical work. Dielectric elastomer actuators (DEAs) have been the gold standard for years (*15*–*19*), because of properties such as their softness, fast response, and high power density. However, these actuators are difficult to scale up, and their membrane form factor complicates integration in robots. Recent electrostatic and electrohydraulic actuators (*20*–*26*) overcome some DEA limitations, gaining robustness and scalability, without compromising high power density. Each class of these actuators works well in specific robotic systems, but substantial reengineering is required when one wants to develop a different application (*27*).

To achieve highly modular and versatile soft actuators, researchers have developed electrically driven fiber actuators (see table S1). DEA fibers (*28*, *29*) are compact and monolithic, yet response time and power density remain below those of biological muscles (50 W/kg). Shape memory alloys (*30*–*33*) exhibit high force density (40 N/g) but slow return times because of cooling time constants (>10 s). They can reach high temperatures (≥50°C) and are made of stiff metals, making the interface with soft materials challenging. Other polymer-based electrothermal actuators show much lower power density and require high temperatures up to 200°C (*34*, *35*). Carbon nanotube–based twisted polymer actuators reach 50 W/kg power density only if operated in an electrolyte bath (*36*). Modular electrically driven actuators with a <20-ms response time and high power density (122 W/kg peak, 57 W/kg average) have recently been introduced with a prismatic form factor and a rigid exoskeleton as part of their body (*37*). There is still a need for highly modular artificial muscles in soft fiber format with power density equal to or higher than that of skeletal muscles. Such soft actuators could enable multifunctional robots with flexible bodies and high-dexterity soft wearable robots.

In this work, we report electrofluidic artificial muscles made of fibers with a power density comparable to that of mammalian muscle (50 W/kg average) that are modular, versatile, and reconfigurable. They are made of antagonistic thin McKibben fluidic actuators driven by electrohydrodynamic (EHD) fiber pumps (*38*) connected in a closed system (Fig. 1A, Movie 1, and movie S1). Electrofluidic fiber muscles (EFMs) have a diameter of 1 to 2 mm, contraction strains of nearly 20%, and response times under 0.3 s. They are directly driven by an electrical input and operate without noise. Figure 1B illustrates the operation of our unitary design: one fiber pump connected at both ends to thin McKibben actuators.

Thin McKibben actuators (Fig. 1C, ii) are power dense, compliant, and have small diameters (<2 mm) (*39*). Their fiber form factor makes them a highly versatile alternative to EM motors for compact, distributed actuation in wearable exosuits and dexterous robots. To date, McKibben actuators have required external pumps and valves,

[1]Tangible Media Group, Massachusetts Institute of Technology, Cambridge, MA 02139, USA. [2]RoboPhysics Laboratory (RPL), Politecnico di Bari, Bari, Italy.
*Corresponding author. Email: vito.cacucciolo@poliba.it (V.C.); ozgun@mit.edu (O.K.A.)

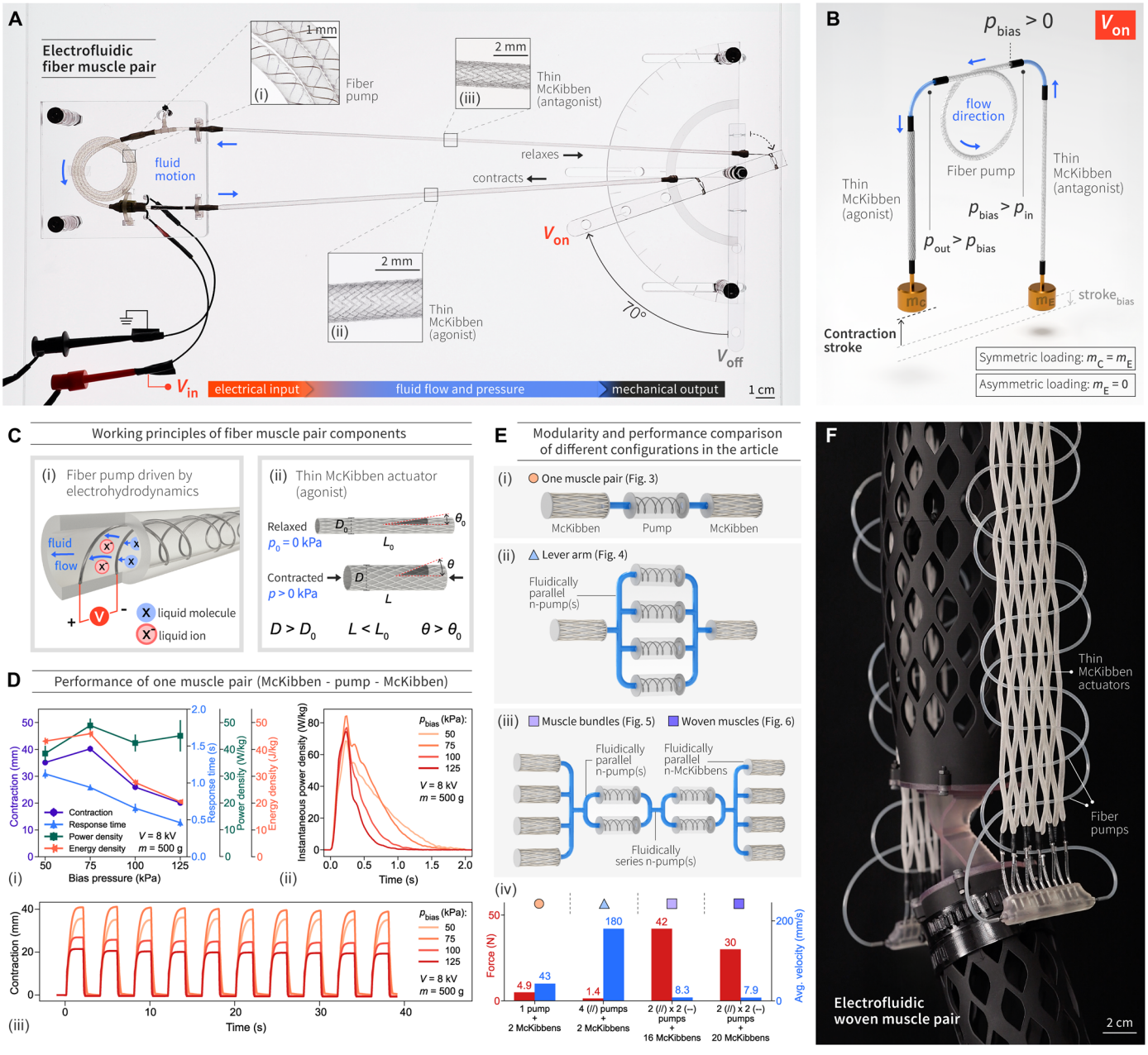


**Fig. 1. EFMs with tunable architecture and performance.** (**A**) Each EFM is composed of two antagonistic thin McKibben actuators (ii and iii) connected by an EHD fiber pump (i), each <2 mm in diameter. Scale bars, 1 mm in (i) and 2 mm in (ii) and (iii). (**B**) Working principle: One fiber pump transfers fluid between an antagonistic pair of McKibben actuators. Filling the system with additional liquid before operation applies a bias pressure that causes both actuators to precontract. When voltage is applied, the agonist actuator contracts, and the antagonist relaxes and extends. Each actuator is connected to a load. Symmetric loading: masses $m_C$ and $m_E$ are equal. Asymmetric loading: $m_E = 0$. (**C**) The muscle converts electrical input into fluid pressure inside the fiber pump (i) and fluid pressure into mechanical output in the McKibben actuators (ii). (**D**) A single muscle pair has an average power density of ≥50 W/kg (asymmetric loading), comparable to that of skeletal muscles (i). Error bars show ± SD for $n = 3$ devices. Instantaneous power density (ii) and contraction (iii) over time versus bias pressure. (**E**) McKibben actuators and pumps can be modularly arranged for different robotic tasks. The simplest EFM (i) consists of one pump and two McKibben actuators (one muscle pair). Multiple pumps in parallel increase velocity (ii); see lever arm demo. Scaling up both the pump and McKibben actuator numbers increases force (iii); see muscle bundle and woven muscle demos. Average force and velocity comparison of different modular configurations in the article (iv). Different forces generated by each configuration are due to the McKibben actuator geometries used (fig. S5B) and operating conditions (figs. S14 and S15). (**F**) Modular scalability allows architected muscles for robotics, including compliant woven muscle pairs on robotic arms. Scale bar, 2 cm.

with few exceptions (*40*), limiting untethered operations. Recently, Smith *et al.* (*38*) introduced charge-injection EHD fiber pumps—millimeter-scale soft tubes with embedded helical electrodes that silently generate pressure and flow without moving parts, solving the long-standing problem of integrating pressure generation in portable systems. We integrated fiber pumps (Fig. 1C, i) with thin McKibben actuators in a closed-circuit antagonistic architecture to realize EFMs. Our EFMs are prefilled with a dielectric fluid, and the

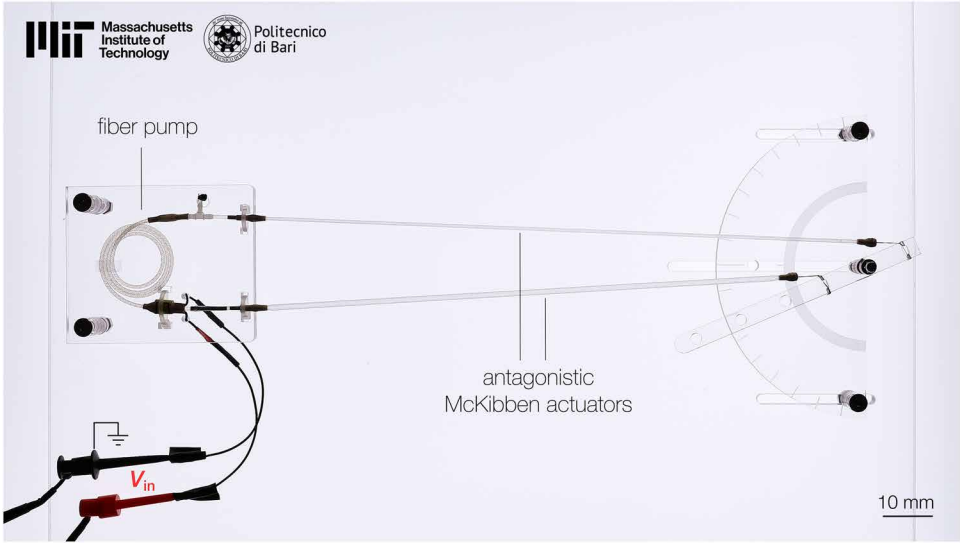


**Movie 1. Overview of EFMs.** Electrically driven fiber muscles deliver a skeletal muscle–like power density (~50 W/kg) and are silent, flexible, and backdrivable. Closed-system operation is achieved by pre-pressurizing the muscle (bias pressure), with an optimal bias value maximizing muscle output. Modularity allows scaling by arranging the pump-to-actuator ratio; demonstrations include a 0.1-s lever throw, a 4-kg lift, and a human-robot handshake.

fiber pumps move the fluid in and out of each McKibben actuator, which contracts or extends in response. These all-fiber-format muscles convert electrical energy from a power supply into fluid pressure in the pumps and then fluid pressure into mechanical work in thin McKibben actuators (Fig. 1A and Movie 1). We used an antagonistic configuration (*41*), similar to skeletal muscles. When our EFM is attached to a joint, the agonist actuator pulls on one side, whereas the antagonist extends as the joint rotates. The result is an EFM that contracts/extends in response to voltage, whose shape and performance can be designed by changing the combination of its two components (McKibben actuators and fiber pumps).

We demonstrated that the performance of these muscles is substantially influenced by the bias pressure applied when prefilling them with a dielectric fluid. The electric field that the closed system tolerates when a bias pressure of 75 kPa is applied is 200% of that without bias (limited by fluid cavitation), resulting in a sevenfold increase in the contraction stroke with the same load (14% versus 2% at a 2-N force). Also, bias pressure enables leveraging the intrinsically nonlinear pressure-stroke response of McKibben actuators, further increasing the stroke at fixed voltage. With a 5-N load, a bias pressure of 75 kPa brings the contraction strain from less than 2% (no bias) to more than 6% (threefold increase) at an applied voltage of 6 kV. At the optimal bias pressure value, our EFMs reach performance comparable to that of skeletal muscles (Fig. 1D).

EFM performance can be programmed by design, simply selecting the number of McKibben actuators to be bundled together and the number of fiber pumps to connect in series and/or in parallel (Fig. 1E). The fiber format makes bundling much simpler than in EM motors. Given that the electrofluidic transducer and the fluidic actuator are decoupled, this adds a second level of versatility, typical of hydraulic transmission and absent in other electrical actuators and skeletal muscle. More actuators in parallel lead to higher forces. A higher ratio of fiber pumps in parallel over fluidic actuators produces a faster response. We demonstrate the versatility of our system through three different robotic demonstrators using the same actuator-pump-actuator ensemble (Fig. 1E): a fast lever (180 mm/s) that launches objects in less than 0.3 s, a muscle bundle that can lift more than 4 kg (200 times its own weight) with 30 mm of stroke (14% strain), and a flat woven muscle (Fig. 1F) that bends a robot arm by more than 40° in less than 2 s and is compliant enough for a human handshake. With their fiber form factor, high power density, and unique modularity, EFMs can fill the need for scalable and versatile fiber-shaped artificial muscles for robotic actuation (*2*, *42*).

## RESULTS

We report a series of results to support our claim that bias pressure is a key requirement to operate fluidic actuators with an integrated pump in a closed system. First, we characterized the performance of the individual muscle pairs (one fiber pump with two McKibben actuators connected in an antagonistic configuration) in terms of force, stroke, and response time. We measured the influence of bias pressure on performance and on the maximum voltage that can be applied to the system. We also developed a model that describes the dynamic coupling of EHD fiber pumps with thin McKibben actuators. This model can be used as a design tool for EFMs in robotic tasks. As input, the model takes the force and response time required by the task and outputs the number and size of the fluidic actuators, the number of fiber pumps, and their series-parallel arrangement. We characterized EFM dynamics and report their stable cyclic operation over 5000 cycles. Last, we demonstrated their modularity with three robotic systems.

### Closed-circuit configuration of EFMs and the importance of bias pressure

To study EFMs as a system, we first characterized their two components: thin McKibben actuators (Fig. 2A) and fiber pumps (Fig. 2B). Details on design, materials, and characterization experiments are in Materials and Methods and in Supplementary Materials and Methods.

We aimed to develop artificial muscles for various robotic applications where compliance, backdrivability, and distributed actuation are important. These applications require a degree of portability and

integration that are hardly compatible with a reservoir open to the atmosphere. Evaporation of the dielectric liquid, leakage risk, and reservoir size for multiple muscles are key limitations of operating electrofluidic muscles in an open-circuit configuration. Therefore, we designed our artificial muscles for closed-circuit operation.

Transitioning from an open- to a closed-circuit design introduced two challenges: storing the dielectric liquid required to fill the McKibben actuators during operation and cavitation near the pump inlet when local pressure dropped below the dielectric liquid's vapor pressure. We addressed both challenges by using antagonistic muscle pairs and filling the system with an additional volume of liquid, increasing its bias pressure above atmospheric pressure.

The configuration and filling procedure are shown in Fig. 2C. Two McKibben actuators are connected to either side of one fiber pump. The system is filled with liquid and then overfilled by an excess volume, resulting in a bias pressure $p_{bias}$. Such bias pressure causes both actuators to contract by a $stroke_{bias}$, determined by the excess liquid volume. EFMs are operated by applying dc voltage to the fiber pump. When the voltage is off, the whole system (pump and two actuators) is at constant pressure $p_{bias}$. When the voltage is turned on, the pump moves liquid from one actuator to the other one. The antagonistic configuration ensures that one McKibben actuator (the extending one) acts as a reservoir for the other (the contracting one). The pressure in the contracting actuator (pump outlet side, $p_{out}$) increases ($p_{out} > p_{bias}$), whereas the pressure in the extending actuator (pump inlet side, $p_{in}$) decreases ($p_{in} < p_{bias}$) until the pressure difference ($p_{out} - p_{in}$) equals the maximum pressure differential generated by the pump at the applied voltage. At this point, the system reaches steady state. The contracted actuator lifted its connected load by a contraction stroke $s_C$ above the $stroke_{bias}$ baseline, producing mechanical work output. The extending actuator elongates by an elongation stroke $s_E \leq stroke_{bias}$. When the voltage is turned off, the pressure difference between the two actuators drives the fluid backward through the fiber pump, which acts as a simple tube in the absence of voltage. Both actuators return to $stroke_{bias}$, and pressure returns to $p_{bias}$. Contraction ($s_C$) and elongation ($s_E$) refer to contraction and extension strokes of the antagonist and agonist McKibben actuators, respectively, each from the pre-pressurized state (bias pressure baseline) to the actuated state.

We tested two loading conditions: symmetric (equal loads on both sides of the muscle pair $m_C = m_E$) and asymmetric (contracting McKibben loaded and extending one unloaded $m_E = 0$) (Fig. 2C). The asymmetric loading condition is used throughout this work to compute the energy and power density of the system, because in this condition, all of the mechanical work done on the lifted load ($m_C$), attached to the contracting actuator, is unambiguously generated by the EFM pair during its contraction phase.

Operating EFMs at their optimal bias pressure has three major implications. Bias pressure increases maximum operating voltage, by preventing cavitation at the pump inlet, which would disrupt operation. It leverages the nonlinear response of McKibben actuators, optimizing pump-actuator matching and increasing the power density output of the system. Bias pressure makes EFMs back-stretchable, increasing their range of motion and enabling compliant interaction with humans and the environment (*43*).

Cavitation refers to the local boiling of a liquid (typically at the pump inlet) when pressure drops below the liquid's vapor pressure. It is disruptive to fiber pumps because it triggers electrical breakdown (the breakdown strength of a vapor at its vapor pressure is markedly lower than the one of the corresponding liquid). For the Novec 7100 dielectric liquid used in this work, the vapor pressure is 27 kPa (absolute pressure) at 25°C (*44*). The total local pressure of the liquid in the pumps is a sum of static pressure (measured by our pressure sensors) and dynamic pressure because of liquid acceleration, which is negative near the emitting electrode. As a result, cavitation can occur when the measured static pressure is at or above the liquid's vapor pressure. Movie S2 shows how cavitation occurs in our system when static pressure drops to a value close to the dielectric liquid's vapor pressure. We demonstrated that cavitation can be prevented by selecting a $p_{bias}$ such that the absolute pressure at the inlet ($p_{in} + p_{atm}$) is always greater than the vapor pressure of the dielectric liquid, with a sufficient safety margin.

We also report how filling the system at an optimal $p_{bias}$ improved its performance both in terms of stroke (operating under load) and response time, leveraging the nonlinear response of McKibben actuators (Fig. 2C, right). Although bias pressure precontraction reduced the total maximum contraction stroke that can be achieved for a given McKibben actuator, the contraction stroke per given finite pressure generated by the fiber pump was higher, because the fiber pump pressure ($p_{pump}$) was applied in the high slope region of the McKibben actuator's pressure-stroke response curve. A similar effect also applies to the volume-stroke response curve of the actuators (Fig. 2A, ii and iii).

We characterized our fiber muscle, composed of two McKibben actuators and one fiber pump, in both open-circuit ($p_{atm}$) and closed-circuit configurations (with $p_{bias} = 75$ kPa) and compared their performances (Fig. 2D). In the closed-circuit configuration, the contraction stroke exceeded the open-circuit stroke for loads on the agonist actuator of greater than 200 g. The closed-circuit configuration also exhibited a faster response across the tested loads. Together, these effects yield a higher power density in the closed-circuit case, and the advantage increased by increasing the applied load, reaching a nearly 250% ratio at a 500-g load (movie S1). The energy density followed the same trend as the contraction stroke: The energy density of the closed circuit with bias pressure exceeded the energy density of the open circuit for loads of greater than 200 g. Methods for calculating the energy density, power density, and other performance metrics are detailed in Supplementary Materials and Methods.

Although performance also depends on the specific fiber pump characteristics and can be improved by using longer, higher-pressure pumps, two important considerations should be highlighted: Longer pumps come at the cost of increased fabrication complexity and power requirements; our model demonstrated that there is a maximum pressure that can be applied to a given pair of closed-circuit McKibben actuators to maximize stroke, because a higher pressure would lead to cavitation, making pump operation impossible (Supplementary Methods).

Adding loads to the McKibben actuators increased the internal pressure of the closed system. We define "initial pressure" as the pressure throughout the system after applying bias pressure and attaching loads. Figure 2E shows measured initial pressures for different values of bias pressure and different loads added to each actuator. This initial pressure determines how much pressure can be applied by the pump before reaching cavitation, the McKibben actuators' active stroke before saturation, and the actuators' burst pressure limit (550 kPa for the actuators used in this work).

In summary, a closed-system design for EFMs provides a practical route toward portability and integration in robotic applications beyond the laboratory. We demonstrated that by filling the system with

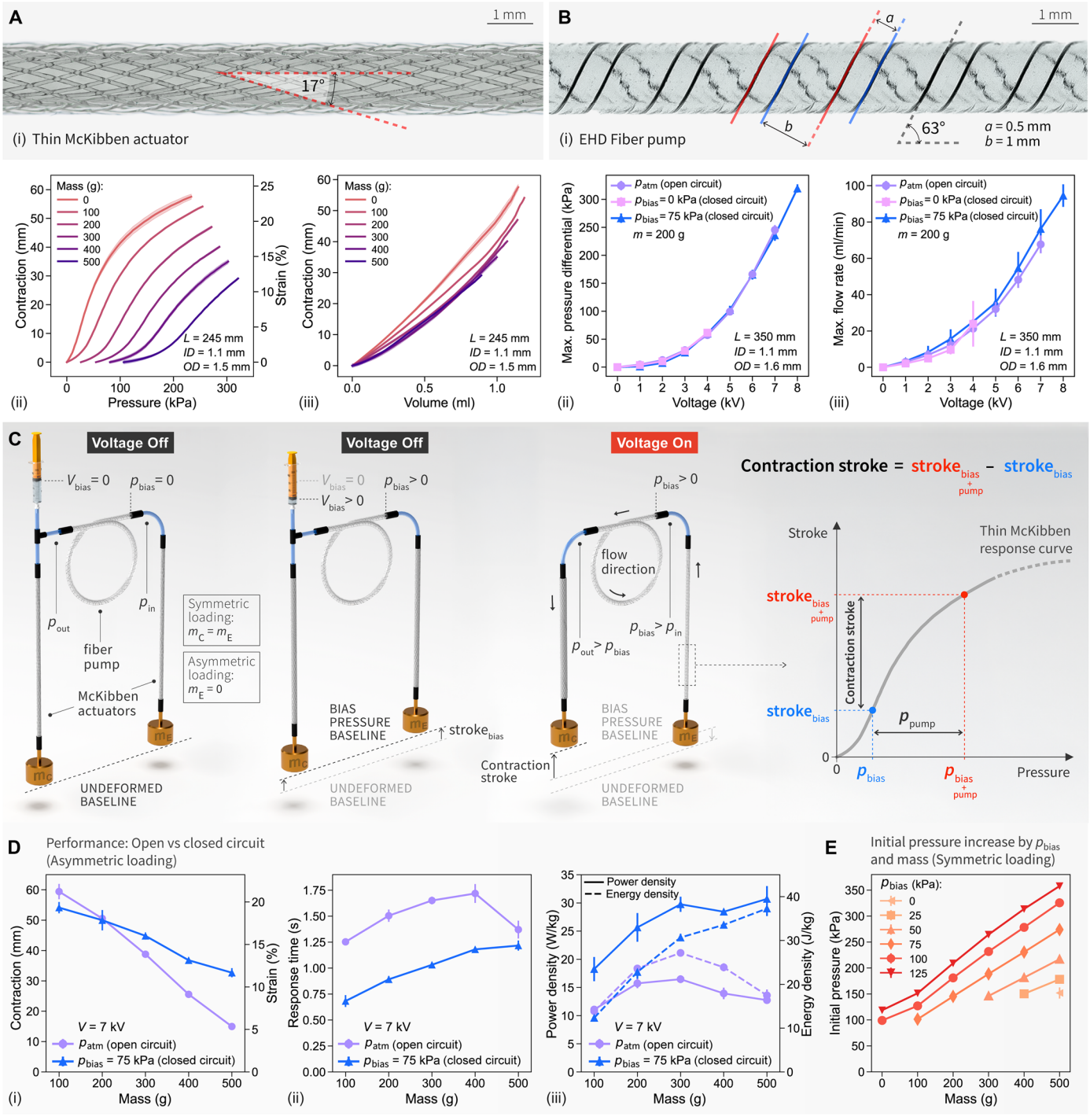


**Fig. 2. EFMs as coupled systems composed of thin McKibben actuators and fiber pumps.** (**A**) Characterization of thin McKibben actuators (ID = 1.1 mm, OD = 1.5 mm, $L$ = 245 mm) showing nonlinear response (i). Contraction $c$ as a function of pressure (ii) and volume (iii). (**B**) Characterization of fiber pumps (ID = 1.1 mm, $L$ = 350 mm) (i). Maximum pressure differential (ii) and maximum flow rate (iii) generated by the fiber pump at different applied voltages under three different fluidic circuit configurations. The performance at the same voltage was unchanged, but the closed circuit at 0-kPa bias pressure showed early breakdown above 4 kV because of cavitation. Scale bars, 1 mm in (A) and (B). (**C**) Two antagonistic McKibben actuators are coupled with one fiber pump transferring liquid between them. By regulating the bias pressure, we leveraged the nonlinear response of the McKibben actuators, improving the contraction stroke and response time for a given pressure and flow rate that the pump generates. (**D**) Applying $p_{bias}$ increased the muscle performance compared with the same muscle operated as an open system at $p_{atm}$ with an external liquid reservoir, especially at higher loads. Contraction (i), response time (ii), power density, and energy density (iii) as a function of the mass attached to the contracting McKibben actuator ($m_C$) at 7 kV. (**E**) Initial pressure of the system changes for given values of bias pressure and because of hanging mass to both muscles (symmetric loading). Shaded areas and error bars represent ± SD over $n$ = 3 devices.

additional liquid until reaching an optimal bias pressure, the performance exceeded that of the same system operated in an open-circuit configuration. The following section presents our physical model and experimental characterization of individual muscle pairs in a closed-system configuration, revealing the optimal bias pressure that maximizes the performance of a given system.

### Physical model of coupled-system dynamics for EFMs

EFMs are electro-fluido-mechanical transducers. They transform electrical power (voltage times current $V \times I$) into fluidic power (flow rate times pressure $Q \times p$) inside fiber pumps and fluidic power into mechanical power (force times velocity $F \times u$) inside McKibben actuators. They operate as a coupled system: The fiber pump response influences the McKibben actuators and vice versa. Therefore, to capture the behavior of EFMs and the effects of key parameters (geometry, materials, and bias pressure), we need a coupled system model (fig. S1).

We modeled thin McKibben actuators by mapping pressure $p$ and volume $v$ inside the actuators to force $F$ and contraction $c$ for a given geometry (diameter, length, and braid angle) and tubing material. The tubing material was assumed to be linear elastic, whereas the braid fibers were assumed to be inextensible.

At a given braiding angle $\theta_0$, the braid uniquely relates the actuator axial $\lambda$ and radial $\lambda_r$ strains as

$$\lambda^2 \cos^2\theta_0 + \lambda_r^2 \sin^2\theta_0 = 1 \tag{1}$$

From Eq. 1, a volume-contraction map is obtained. Given that the only free kinematic variable is the $c$, the actuator pressure can be related to $c$ by minimizing the difference between elastic energy $E_{elastic}$ and external work $p \times v + F \times c$,

$$\min_c \left(E_{elastic}(c) - pv(c) - Fc\right) \rightarrow p = p(c, F) \tag{2}$$

This relation can be inverted to obtain the actuation force as a function of pressure and contraction. The force scales with the cross-sectional area of the McKibben actuator, $\pi d_0^2/4$, as

$$F = F\left(c, p\right) = \pi d_0 \left(h_0\, B(c) + \frac{d_0\, C(c)\, p}{4}\right) \tag{3}$$

where $d_0$ and $h_0$ are the tubing diameter and thickness. Here, $B(c)$ and $C(c)$ are two functions of $c$ and depend on the tubing material and braiding angle as detailed in the "Thin McKibben actuator model" section of Supplementary Methods. The actuator pre-pressurization is accounted for by introducing an offset (bias) contraction, corresponding to a bias pressure and bias volume.

To model fiber pump behavior, we used experimental pressure–flow rate characteristic curves obtained as a linear fit between the maximum pressure difference $\Delta p_{max}$ between output and input of the pump (obtained at zero flow rate) and maximum flow rate $Q_{max}$ (at minimum pressure differential), at each given voltage $V$

$$Q = Q_{max}(V) - \frac{Q_{max}(V)}{\Delta p_{max}(V)} \Delta p \tag{4}$$

Fiber pump behavior has been reported to be close to linear (*38*), so a linear fit maps it well. A physical model for fiber pumps, accounting for the multiphysics, multiscale set of mechanisms, is still an open research topic and goes beyond the scope of this work.

We coupled fiber pump response with the McKibben actuator model by equating the pump flow rate to the rate of change of fluid volume inside the McKibben actuators. The total liquid volume in the system stays constant, equal to the internal volume at rest plus bias volume (continuity). The pressure difference generated by the pumps is equal to the difference between the pressure in the agonist and antagonist McKibben actuators $\Delta p = p_{agonist} - p_{antagonist}$. The pressure inside each actuator is correlated to its $c$. Using Eq. 4 and setting the coupling conditions listed above, we obtained a coupled system model that predicts the dynamic interaction between fiber pumps and McKibben actuators under specific load and voltage conditions.

We validated the model experimentally, so that it can be reliably used as a design tool for EFMs beyond the ones tested in this article. The model outputs shown in Fig. 3E and fig. S2 are derived from the full numerical solution of the physical model. Here, we derive simplified solutions to define scaling laws for preliminary design. Below, we report two useful formulas, whose derivation is detailed in the "Modular muscle architectures" section of Supplementary Methods.

Given a single fiber pump module with characteristic maximum pressure $\Delta p_{max}$ and maximum flow rate $Q_{max}$, the overall maximum pressure in the EFMs is proportional to the number of pumps in series $N_-$. The maximum flow rate scales with the number of pumps in parallel $N_{\|}$. Using $N_{act}$ identical McKibben actuators per agonist and antagonist sides, the muscle response time can be approximated as

$$\tau = \frac{N_{act}\, \pi\, d_0^2\, l_0}{4\, N_{\|}\, Q_{max}} \tag{5}$$

where $d_0$ and $l_0$ are the initial diameter and length of the actuators. In short, the response time decreases as the number of fiber pumps in parallel increases, whereas it increases proportionally with the size and number of McKibben actuators. Thinner and fewer McKibben actuators yield a faster response for a given set of fiber pumps.

The steady-state muscle contraction strain $\varepsilon_{max} = s_c/l_0$, resulting from the maximum pressure differential $\Delta p_{max}$ generated by each fiber pump at a given voltage, can be estimated as

$$\varepsilon_{max} \approx \sqrt{\frac{N_-\, \Delta p_{max}\, d_0/h_0}{4\mu\left(\frac{1}{\sin^2\theta_0} - 2\right)}} \tag{6}$$

where $h_0$ and $\mu$ are the thickness and shear modulus, respectively, of the McKibben actuator tubing material. Equation 6 shows that the steady-state contraction increases with the square root of the number of pumps in series. The strain is kinematically limited by the braid geometry, which imposes an upper bound on the maximum contraction that can be achieved, regardless of the pump-generated pressure, $\varepsilon_{max} \leq \frac{1 - \left(\sqrt{3}\cos\theta_0\right)^{-1}}{2}$ (see fig. S2G). It is important to highlight that Eq. 6 holds for unloaded muscles. The higher the force generated by the muscles is, the higher the $\Delta p_{max}$ required to reach a given $\varepsilon_{max}$. Together, Eqs. 3, 5, and 6 provide a simple yet powerful design tool for EFMs to meet requirements given by the robotic task (force, response time, and strain). All of the details of the model derivation and experimental validation are provided in Supplementary Methods and figs. S1 and S2.

### Characterization of individual pairs of EFMs

We characterized the quasi-static and dynamic response of EFMs under load at different bias pressure values. McKibben actuators were tested with their top ends attached to a vertical plate and their

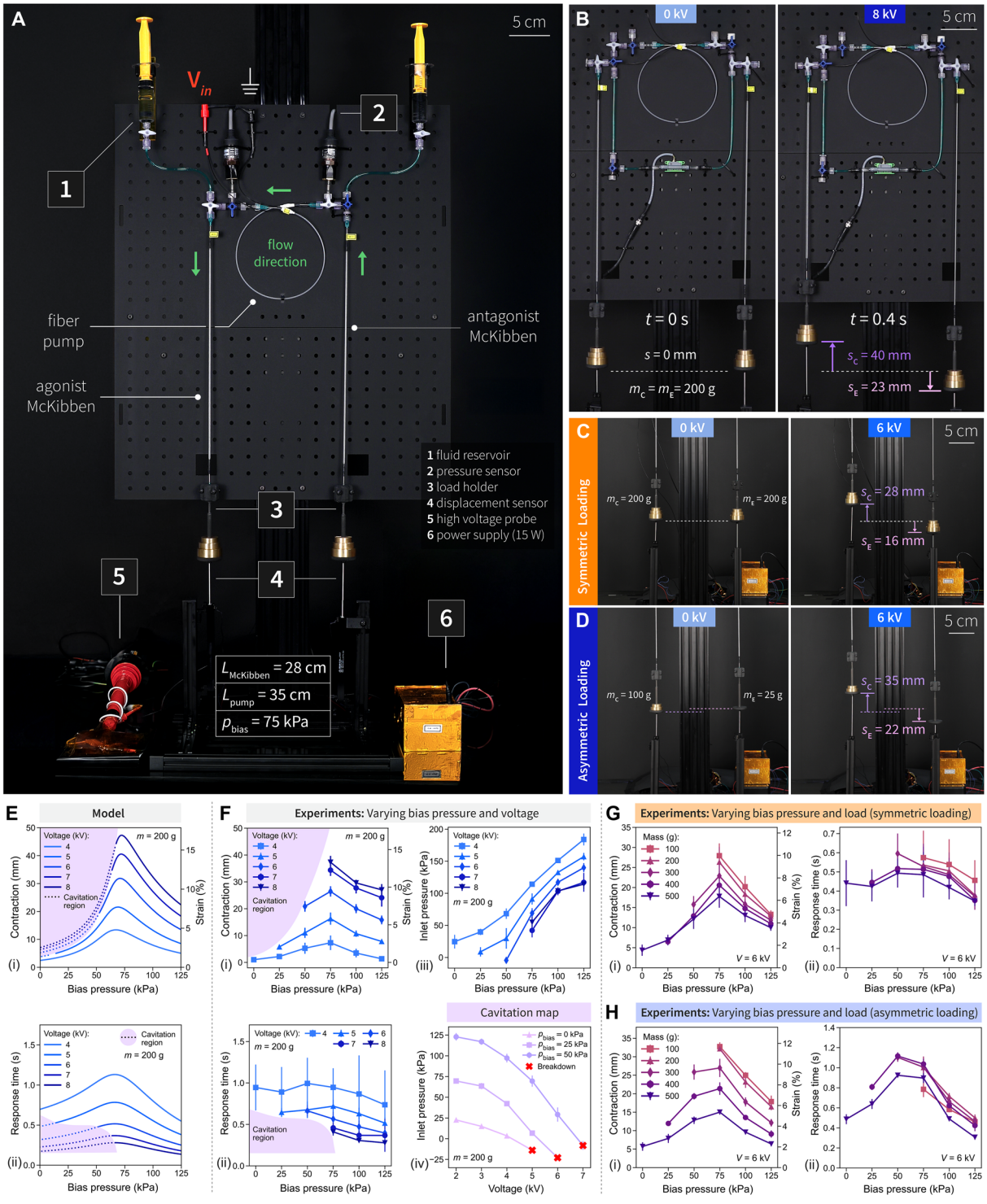


**Fig. 3. Characterization of individual muscle pairs.** (**A**) Experimental setup consists of two fluid reservoirs, two gauge pressure sensors at the pump inlet and outlet, two load holders, two displacement sensors, a high-voltage probe, and a 15-W high-voltage power supply. (**B**) Muscle response at 8 kV under 200-g symmetric loading: $s_C = 40$ mm (agonist) and $s_E = 23$ mm (antagonist) in 0.4 s. Actuation tests at 6 kV under (**C**) symmetric loading (200 g on each actuator) and (**D**) asymmetric loading (100 g on contracting actuator only). (**E**) Model prediction for contraction (i) and response time (ii) and (**F**) experimental results for contraction (i), response time (ii), and inlet pressure (iii) for different bias pressures, at voltage values ranging from 4 to 8 kV, under a fixed symmetric load of 200 g. Pressure measured at the pump inlet (iv) that correlates to the cavitation regions shown in (i) and (ii). When gauge pressure decreases below 0, there is a high risk of cavitation, and pumps cannot be operated (movie S2). Contraction (i) and response time (ii) at 6 kV under different bias pressures and applied mass ranging from 100 to 500 g under (**G**) symmetric loading and (**H**) asymmetric loading. All values with error bars correspond to mean ± SD for $n = 3$ devices. Scale bars, 5 cm for (A) to (D).

bottom ends attached to load holders connected to linear displacement sensors (Fig. 3A, fig. S6, and Supplementary Materials and Methods). Three-way valves connected the actuators to the fiber pump and to experimental accessories: two syringe reservoirs (for filling the system and removing air bubbles) and two pressure sensors placed at the pump inlet and outlet. During testing, the valve positions ensured that the muscles were disconnected from the syringes and connected to the pressure sensors. Voltage was applied to the fiber pump using a compact 15-W high-voltage power supply (0 to 10 kV) and monitored with a high-voltage probe.

When voltage is applied, the fiber pump transfers fluid from the antagonist actuator (which extends) to the agonist actuator (which contracts), lifting the load. Figure 3B shows snapshots of the muscle pair at rest (left) and under steady actuation at 8 kV (right). After a 0.4-s transient, the agonist actuator contracted by 40 mm, lifting a 200-g load, whereas the antagonist extended by 23 mm. Movie S3 shows the operation of the experimental setup with live measurements.

We tested symmetric (equal loads on both sides of the muscle pair $m_C = m_E$) and asymmetric (contracting muscle loaded and extending one unloaded $m_E = 0$) loading conditions (Fig. 3, C and D). The symmetric loading condition was used for the physical model. Even in the symmetric loading condition, the net mechanical work generated by the contracting actuator during one actuation half-cycle was nonzero. Only a fraction of the potential energy lost by the load $m_E$ connected to the extending actuator was transferred through pressure energy to the contracting actuator and the lifted load; most of it dissipated.

### *Bias pressure and voltage dependence under constant load: Model validation and experimental results*

The physical model described in the previous section and Supplementary Methods was used to estimate the steady-state contraction and response time of EFMs at different voltage and bias pressure values (Fig. 3E). To validate the model, we conducted experiments under the same conditions using the setup in Fig. 3. Both actuators were loaded with 200 g. Voltage ranged from 4 to 8 kV in 1-kV steps, and bias pressure ranged from 0 to 125 kPa in 25-kPa increments. For each condition, voltage was stepped from 0 to set value, and the response time was measured as the time to reach from 0 to 90% of the agonist contraction.

The results show that the model accurately predicts EFM response, generating a map that closely matches the experimental data. The model is fully physical: All parameters were based on physical quantities, and no fitting multipliers were added. Discrepancies in peak strain and response time at low bias pressures were attributed to the model's simplicity, which excludes tube-braid friction in the McKibben actuators and viscoelastic expansion of the fiber pump and three-way valves under pressure, load, and liquid inertia. These approximations keep the model simple to interpret and apply. Overall, the model agrees well with experimental results across a wide operational range of EFMs, supporting its validity.

The results show that the steady-state contraction of EFMs increases by increasing the voltage applied to the fiber pump, whereas the response time decreases for a fixed bias pressure. Consistent with prior EHD and fiber pump literature, a higher voltage leads to both a higher maximum pressure and a higher flow rate (*38*, *45*).

At a fixed voltage, both model and experimental data show that the steady-state contraction stroke and strain are maximized for a bias pressure of 75 kPa, and this optimum remains constant across the tested voltage range. We identified and demonstrated the existence of an optimum for bias pressure. This optimum results from shifting the application range of the fiber pump–generated pressure toward a steeper region in the McKibben actuators' response curve [Fig. 2, A (ii) and C]. As bias pressure increases, response time initially increases slightly and then decreases. This trend is linked to the contraction-stroke response: For a given contraction velocity of the muscle, the response time is longer if the steady-state contraction is larger. The response time variation with bias pressure is smaller than the contraction variation.

A critical effect captured by both our model and experimental data is the existence of a cavitation region where EFMs cannot be operated. The use of bias pressure allowed applying the full voltage range that the fiber pump can be operated at, thus enabling the whole performance of EFMs. At zero or low bias pressure values, voltages above 4 kV generated cavitation at the pump inlet, leading to electrical breakdown of the pumps. Using the optimal bias pressure of 75 kPa, or higher pressures, the system operated stably up to 8 kV, leading to an increase in contraction stroke of 37 times (37 mm versus 1 mm) and a reduction in response time of more than 50% (from 1 s to <0.4 s). With a 200-g load and an optimal bias pressure of 75 kPa applied, a pair of EFMs at 8 kV achieved a contractile strain of >14% (stroke of 40 mm) in 0.4 s (movie S3).

To further investigate cavitation and how bias pressure affects it, we measured the fiber pump inlet pressure across different values of bias pressure and applied voltage. Figure 3F (iii) shows how pressure at the pump inlet, for a given applied voltage, increased with increasing bias pressure. For a given bias pressure, increasing voltage led to a lower inlet pressure. The reported inlet pressures corresponded to the values reported in Fig. 3F (i) and (ii). It should be noted that the measured inlet pressures exceeded the filling bias pressure because of the added mass (see Fig. 2E). When voltage was applied, the inlet pressure decreased and the outlet pressure increased. A higher voltage led to a lower pressure at the inlet and a higher pressure at the outlet. The cavitation map in Fig. 3F (iv) shows inlet pressure curves for each bias pressure value. Cavitation occurred when the voltage increased enough for the inlet pressure to drop below atmospheric pressure (gauge $p < 0$), triggering electrical breakdown (movie S2). The cavitation threshold shifted higher with increasing bias pressure (Fig. 3F, i).

### *Bias pressure and load dependence at fixed voltage*

Figure 3 (G and H) shows the steady-state contractions and step response times of EFMs under varying bias pressures and applied loads. As discussed earlier, increasing the load connected to the actuators increased the initial pressure, in addition to bias pressure. Thus, the muscle could operate at a low or even zero bias pressure when a high load was added to the actuators.

Figure 3G presents data for the muscle loaded symmetrically. Contraction and response time showed similar trends to those in Fig. 3F, with contraction peaking at an optimal bias pressure of 75 kPa, independent of the applied load. This counterintuitive phenomenon results from a combination of opposing effects: Greater loads increase initial pressures for a given bias pressure; increasing load shifts the high-response region of the McKibben contraction-pressure curve toward higher pressures (Fig. 2A, ii). These two effects balance out, yielding a constant optimal bias pressure of 75 kPa across tested loads (100 to 500 g). For a given bias pressure, increasing the load decreased both the contraction and response time.

Figure 3H reports the same tests but with the muscle loaded asymmetrically. Loads from 100 to 500 g were applied to the contracting

actuator only, whereas the extending actuator was left unloaded. The overall trends of contraction and response time dependencies with bias pressure are also shown for asymmetric loading. Contraction, strain, and response time did not differ appreciably from those in the symmetric loading case. Response times were on the order of two times longer, because the mass on the extending actuator in the symmetric case partially contributed to lifting the load on the contracting actuator through pressure energy.

### Rapid actuation: Four fiber pumps connected in parallel driving two McKibben actuators

EFMs, operating under optimal bias pressure, exhibited a performance that enabled dexterous robotic applications. The performance could be tuned by selecting the number of fiber pumps and McKibben actuators arranged in each muscle. To achieve fast response, we connected four fiber pumps fluidically in parallel to an antagonistic pair of McKibben actuators. A high ratio of pumps in parallel to actuators led to high flow transfer into the actuators in a short time. The resulting muscle response was fast enough to launch objects when connected to a lever arm (Fig. 4A, fig. S13, and movie S5).

Arranging multiple pumps in parallel effectively increased the flow rate and instantaneous power density in the system. When we apply an 8-kV voltage step, the agonist actuator contracted fully in 0.13 s, achieving a contraction rate of 180 mm/s [Fig. 1E (iv) and fig. S14]. We added a stopper to block the lever arm when it reached a horizontal position. The arm rapidly launched a table tennis ball 24 cm into the air (Fig. 4B). Movie S6 and Fig. 4C show the lever arm response throwing a series of objects, namely, a table tennis ball, cherry tomato, and brussels sprout, and flipping a fried egg prop and toy figurines.

### Electrofluidic muscle bundles for scaling up forces: Two parallel–two series pumps driving an antagonistic eight–McKibben bundle actuator pair

We bundled fluidic muscles to demonstrate scalable force generation by increasing the number of McKibben actuators in parallel, following design principles of Suzumori *et al.* (*46*, *47*), analogous to mammalian muscle architecture. Each muscle pair consisted of two identical antagonistic bundles. Each bundle was made of eight thin McKibben actuators [inner diameter (ID) = 1.25 mm, outer diameter (OD) = 1.75 mm] arranged in a circular geometry, with two fiber pumps wound around them [OD = 7 mm, length ($L$) = 280 mm] (Fig. 5A and movie S7). McKibben actuators on each side were arranged in a fluidically parallel configuration, sharing the same fluidic input. Two fiber pumps on each side were also configured in parallel, increasing the flow rate. The two bundles were then fluidically connected in series, forming a closed fluidic circuit (Fig. 5B, fig. S13, and Supplementary Materials and Methods). In this series configuration, the pressure differential generated across each muscle is the sum of the ones generated by each pair of pumps in parallel. The resulting device is a light, flexible, and compact robotic muscle weighing 22 g (16 McKibben actuators plus four fiber pumps, with liquid), capable of lifting 200 times its own weight (4 kg plus 250 g of preload) and achieving a 30-mm contraction (11% strain).

Muscle bundles were tested under two loading configurations—symmetric and asymmetric—at a bias pressure of 135 kPa, which was selected on the basis of model-predicted optimal bias pressure and to prevent cavitation (fig. S15). Figure 5C shows the pair in asymmetric loading configuration (only the contracting muscle is loaded). When voltage was applied to the four pumps (electrically in parallel), the agonist bundle contracted, lifting 2.25 kg through a 39-mm stroke, whereas the antagonist extended. Long-term cyclic operation (Fig. 5D) showed stable performance over 1000 cycles at 0.5 Hz under 1 kg per bundle with 6-kV applied voltage.

Figure 5E shows the electrofluidic muscle bundle characterization. Under preload, the bundle contracted by 32 mm in 1.2 s, with a pump-generated pressure of 400 kPa at 7 kV (Fig. 5E, i). With a load of 3 kg per muscle, it contracted by 27 mm in 1.8 s at 7 kV (Fig. 5E, ii). Asymmetric loading showed a 30% increase in contraction and a longer response time. Figure 5E (iii) and movie S8 show lifting loads up to 4 kg at 7 kV. Figure 5E (iv) compares symmetric and asymmetric loading.

### Electrofluidic woven muscles: Showing backdrivability in a human-robot handshake

A key advantage of 1-mm fiber muscles is that we can intertwine them into textiles. To demonstrate this capability, we fabricated flat textile muscle pairs by weaving McKibben actuators and fiber pumps together (Fig. 6A). The resulting woven muscles are flexible and can be integrated into textile exosuits that offer muscular support. Their design is highly modular: The number of McKibben actuators in parallel sets the load capacity of the muscle, and the ratio between the number of McKibben actuators and fiber pumps in parallel sets the response time. The woven muscle consisted of 10 parallel McKibben actuators (ID = 0.7 mm, OD = 1 mm) forming the warp and two fluidically parallel fiber pumps interwoven as the weft (Fig. 6A and fig. S13). A 40-cm-long bare thermoplastic polyurethane (TPU) extension tubing was added to each pump to span the entire muscle length. The resulting woven muscle was 40 cm long and 6 cm wide (movie S9 and Supplementary Materials and Methods).

We demonstrated the electrofluidic woven muscles as biceps-triceps pairs of a three-dimensional printed, human-scale robotic arm (Fig. 6B). Woven muscles can be easily bent, folded, twisted, and stretched (movie S9). When operated under bias pressure, they remained compliant and intrinsically back-stretchable in all configurations. We demonstrated this important feature in a human-robot handshake (Fig. 6C and movie S10). The muscles drove the robot arm to a handshake position, and a human could naturally shake it because both muscles easily deformed: The biceps went slack, and the triceps stretched. As demonstrated by years of research in legged robotics, backdrivable actuators are essential for enabling agile robots (*48*). Common EM motors in robots are not backdrivable because of the high gear ratio required to achieve high torque at small sizes. Although large-radius EM motors and additional mechanisms have been used for backdrivability, they are often too bulky for wearables (*49*). McKibben actuators alone require extra components to allow back-stretchability at rest (*43*). With bias pressure, our electrofluidic muscles offer intrinsic compliance and back-stretchability across their operating conditions (movie S11).

Figure 6 (D and E) shows woven muscle characterization on the robotic arm. We selected a bias pressure of 120 kPa on the basis of model-predicted optimal bias pressure for this configuration (105 kPa) to prevent cavitation and to stay below the thin McKibben actuator's burst pressure of ~550 kPa (fig. S15). We used a higher bias pressure in the bundle and woven muscle demonstrations than the optimal value for the muscle pair (75 kPa; Figs. 2 and 3), because these demonstrations used thinner actuators and two pumps connected in series (Fig. 6B).

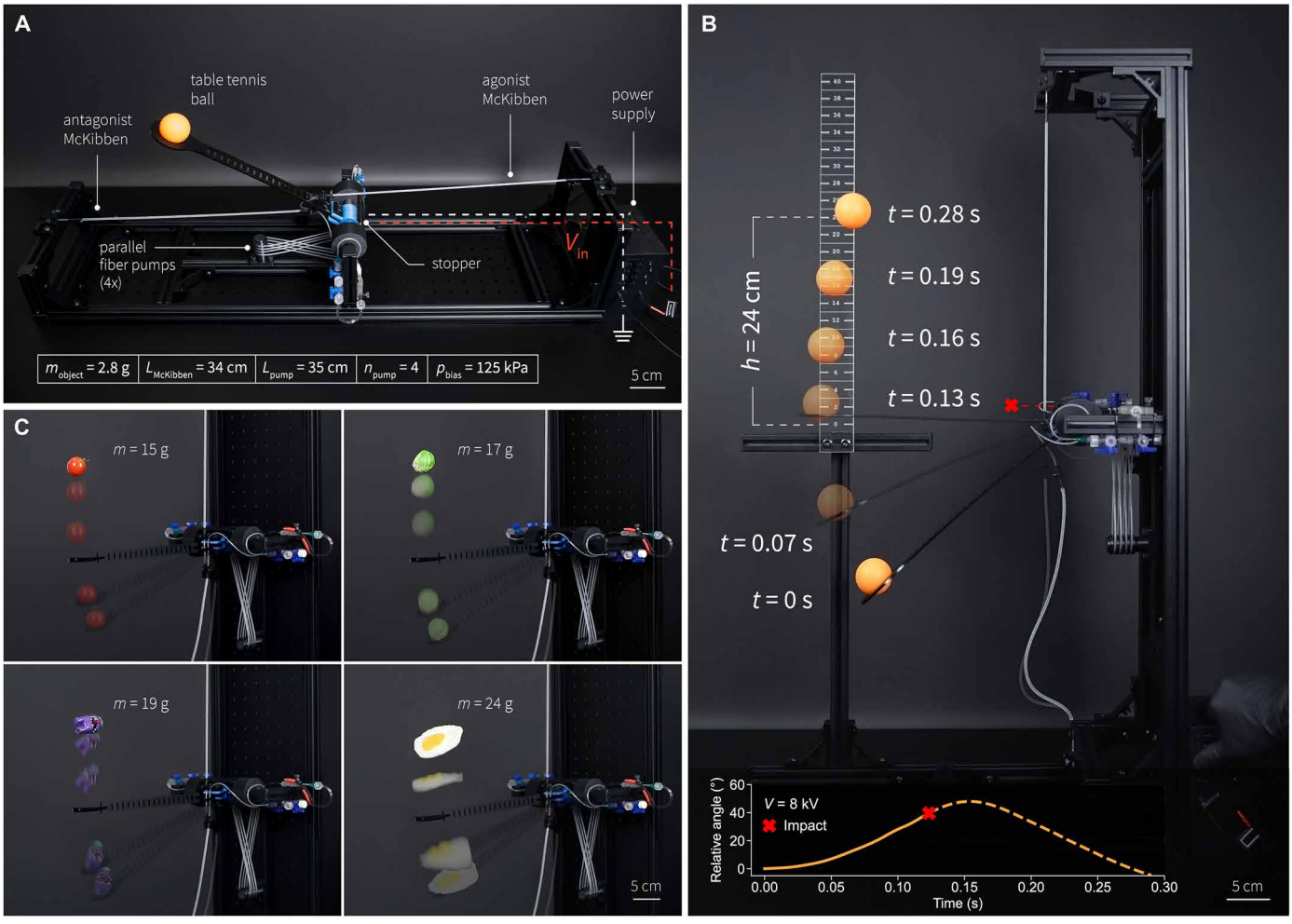


**Fig. 4. Four fiber pumps connected in parallel demonstrating rapid actuation.** (**A**) A lever arm/catapult setup was connected to an antagonistic pair of McKibben actuators and four fiber pumps arranged fluidically in parallel configuration to increase flow rate and hence shorten response time. (**B**) When 8 kV was applied to the muscle, the agonist actuator contracted rapidly within 0.13 s, driving the lever arm into the horizontal stopper and launching the table tennis ball 24 cm upward in <0.3 s. Time measurements start from the onset of muscle contraction ($t$ = 0 s). (**C**) Everyday objects of various masses (<25 g) were rapidly launched into the air. Scale bars, 5 cm.

Figure 6D shows the bending response of the robotic arm driven by the woven muscle pair without additional mass (forearm $m$ = 350 g). By increasing the voltage to 8 kV, the arm bent by 42° in 3.2 s at a pump-generated pressure differential of 460 kPa (movie S10). Figure 6E shows tests at a fixed voltage (8 kV) with variable loads up to 600 g. Under a 600-g mass, the biceps muscle generated 30 N of force (fig. S14).

This woven setup exhibited a slower response than the individual muscle pairs and the lever arm because of the lower ratio of fiber pumps in parallel to the McKibben actuators. We demonstrated that the response time can be tuned by adjusting this ratio in the woven muscle. Figure 6F and movie S10 show the system response when varying only the number of McKibben actuators in the biceps. Reducing the number of actuators from 10 to 2, while keeping the same number of pumps, reduced the response time from >3 to 1 s, with only a small reduction in bending angle. Although the bending angle would eventually decrease at higher loads with fewer actuators, this result highlights that tuning the actuator-to-pump ratio enables the response time to be matched to application requirements.

## DISCUSSION

Here, we report EFMs, a class of electrically driven soft fiber actuators. A dielectric liquid is pressurized by 1- to 2-mm-thick fiber pumps and transferred into thin McKibben actuators, producing contraction. We studied and designed the operation of these muscles as a closed system: By using an antagonistic configuration and an optimal bias pressure, it is possible to eliminate liquid reservoirs, improve performance, and prevent cavitation. We report the use of these muscles in untethered robotic systems, whose shapes, sizes, and performances are designed by selecting the number of actuators, pumps, and their arrangements. Our robotic systems generate large forces (>4 kg) and fast responses (<0.3 s), with average power densities exceeding 50 W/kg.

We believe that the findings of this work not only validate the effectiveness of the proposed EFMs in the specific context studied but also underscore their broader potential across a wide spectrum of future applications. In particular, these EFMs could be adapted and extended to enhance the functionalities, adaptabilities, and performances of other soft robotic systems and be integrated into

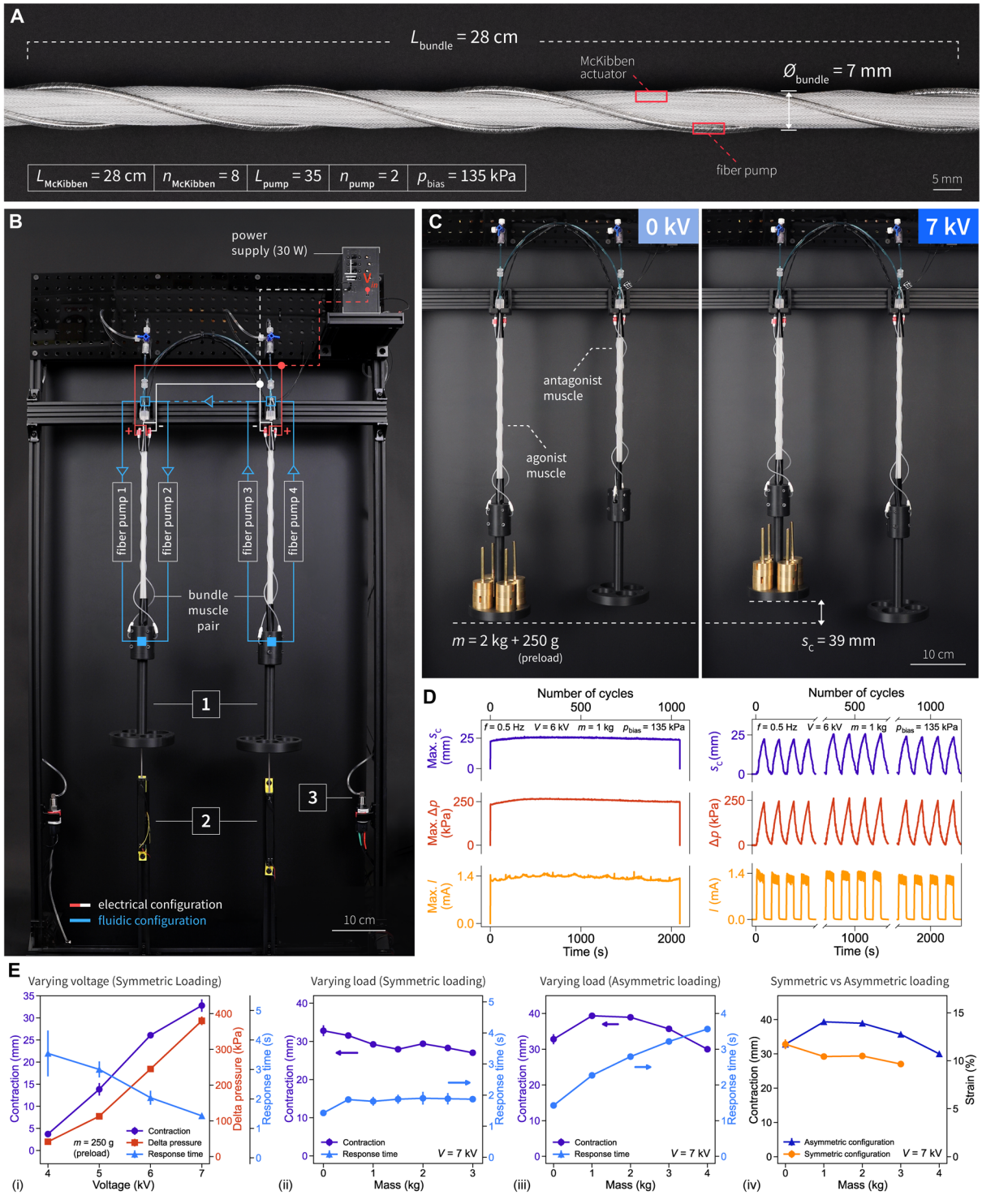


**Fig. 5. High-force electrofluidic muscle bundles lifting a load of more than 4 kg.** (**A**) Close-up of one muscle bundle consisting of two fiber pumps ($L$ = 350 mm) wound around eight McKibben actuators ($L$ = 280 mm). (**B**) Electrical and fluidic configurations of a muscle bundle pair arranged to scale up force generation in a compact form factor. The characterization setup included two load holders, two displacement sensors, and two gauge pressure sensors monitoring inlet and outlet pressures. (**C**) Muscle bundle under a 2-kg (+250 g preload) asymmetric load, contracting by 13.6%. (**D**) Cyclic stability test for 1000 cycles at 0.5 Hz, lifting 1 kg (+250 g preload) on each bundle at 6 kV and 135 kPa of bias pressure. Contraction ($s_C$), delta pressure ($\Delta p$), and current ($I$) over time. Maximum currents evaluated after applying a low-pass filter (cutoff frequency: 10 Hz) on the raw data. (**E**) Muscle performance under symmetric loading with voltage varying between 4 and 7 kV (preload) (i); contraction and response time versus additional mass (ii); under asymmetric loading, contraction and response time versus additional mass (iii); comparison of contraction and strain between symmetric and asymmetric loading conditions (iv). Values with error bars correspond to mean ± SD for 10 cycles. Scale bars, 5 mm in (A) and 10 cm in (B) and (C).

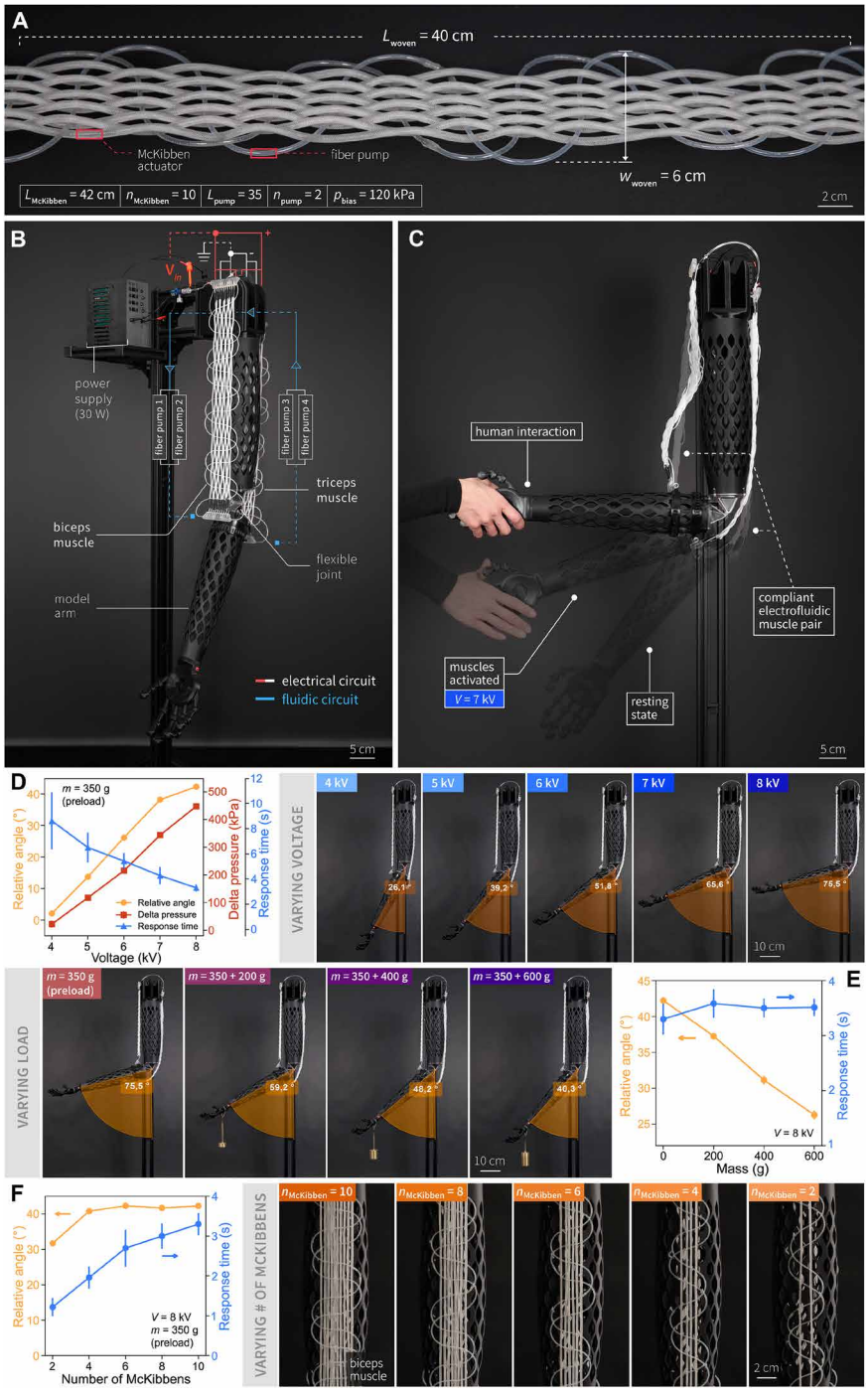


**Fig. 6. Electrofluidic woven biceps and triceps muscles showing backdrivability in a human-robot handshake.** (**A**) Close-up of one woven muscle consisting of two fiber pumps ($L$ = 350 mm) woven with 10 McKibben actuators ($L$ = 420 mm). After weaving the actuators and pumps together, the woven muscle length was 40 cm and the width was 6 cm. (**B**) Electrical and fluidic configurations of a woven biceps and triceps muscle pair driving a human-scale forearm model. The forearm (preload) weighed 350 g. (**C**) Fluidic muscles are compliant and backdrivable, enabling smooth human-robot interaction. (**D**) Arm bending is proportional to the applied voltage at a fixed load. (**E**) The muscle lifts up to 600 g of additional mass with a relative bending angle of 26° at 8 kV. (**F**) Demonstrating scalability and modularity: Reducing the number of McKibben actuators in the biceps from 10 to 4 shortens the response time by 42%, without a notable change in the relative bending angle (>40°) at fixed load. For the whole figure: Values with error bars correspond to mean ± SD for 10 cycles, the applied bias pressure is 120 kPa, and relative angle refers to the difference between the final angle of the arm in the active state and the initial angle at rest. Scale bars, 2 cm in (A) and (F), 5 cm in (B) and (C), and 10 cm in (D) and (E).

emerging wearable devices, where flexibility, lightweight design, and responsive actuation are critical.

## Voltage levels and safety considerations

The fiber pumps in our EFMs are electric field–driven transducers, which operate at high voltage (3 to 8 kV) and low (<1 mA) current. Similar to other electrostatic actuators such as DEAs and electrohydraulic zipping actuators, reducing the diameter and interelectrode gap can reduce the required voltage. The voltage and current levels used in this work are already within safe limits for humans, provided that reasonable caution is exercised and power electronics comply with industry safety standards. Our actuators are operated by voltage converters with a short-circuit current that is limited by the converter impedance (which is much higher than that of the human body). A typical fiber pump operating at 7 kV and <1 mA can be driven by a converter with a ≤1-mA short-circuit current. This current is well below the human safety threshold of 20 mA (*50*). On the contrary, if the pump voltage was reduced, for example, to 300 V, then for the same power output, the current would need to increase to >23 mA, a value that exceeds human safety limits. Therefore, keeping the voltage above 1 kV is desirable.

In addition to safety, using high voltage and low current has advantages in terms of power distribution when scaling from individual actuators to full-scale robotic systems with tens of actuators. Low currents keep losses low and enable very thin wiring, reducing overall system mass (fiber pump and electrical wire weights are comparable) and bulk. A trend toward high voltage (up to 800 V) and low current has recently emerged in the electric car industry to speed up charging (*51*). For EFMs, we expect that electrical currents will be further reduced by increasing efficiency in future research. Power electronics will be designed with safety features and including separate high impedance power lines driving each pump. More details on voltage and safety are provided in the Supplementary Materials.

## Limitations and future directions

Some limitations for practical deployment of EFMs remain. The main limitation is the <3% energy efficiency of the fiber pumps (fig. S7A), which is due to a limited understanding of the EHD mechanism. Consequently, the overall efficiency of the EFM is <2.5% (fig. S7C).

The working fluid used in this work, 3M Novec 7100, is a commercially available hydrofluoroether (HFE); however, this fluid is

supplied by only one manufacturer and faces supply and environmental constraints. Luo *et al.* (*52*) reported the use of nonfluorinated liquids in EHD fiber pumps with performances that can match or exceed those of HFE-based ones. There is both a need and an opportunity to study alternative liquids (*53*, *54*), including tailoring their key properties—such as viscosity and permittivity—through blending or additives (*55*), while accounting for polymer and electrode compatibility. Previous research (*54*, *56*) empirically identified criteria for liquids that work well for EHD pumping and referred to them as electroconjugate fluids. Exploring alternative fabrication methods for fiber pumps (*57*, *58*) could improve throughput and broaden adoption. A deeper understanding of EHD and access to a wider range of commonly available fluids will enable EFMs to power future generations of highly dexterous robots.

## MATERIALS AND METHODS

### McKibben actuator materials and fabrication

McKibben actuators were composed of an internal elastomer tube and an outer braid that guides its deformation (fig. S5, A and B). We fabricated our actuators using TPU tubing, with Shore 40A hardness and a wall thickness of 0.2 mm. TPU was chosen over the more widely used silicone rubber because of its compatibility with the fluorinated dielectric oil used in fiber pumps. The outer braid was composed of 100-μm-thick nylon monofilaments ($n = 24$) with an initial braid angle of 17° (Fig. 2A, i).

### Fiber pump materials and fabrication

Fiber pumps used in this study were based on the design and fabrication method presented by Smith *et al.* (*38*). The pumps we fabricated have a shorter electrode distance (0.5 mm) and a slightly larger helix angle (63°). Fiber pumps were fabricated via filament winding using platinum electrodes (75 μm in diameter) and TPU 95A monofilaments, forming a double-helix structure with 0.5-mm electrode spacing (figs. S3 and S4). All pumps had an ID of 1.1 mm, an OD of 1.6 mm, and an $L$ of 350 mm. Figure 2B shows (i) a close-up image of one fiber pump, with the spiral-shaped electrodes visible and (ii and iii) characterization of three samples with ID = 1.1 mm, OD = 1.6 mm, and $L = 350$ mm. For all of the experiments, 3M Novec 7100 (methoxy-nonafluorobutane $C_4F_9OCH_3$) was used as the dielectric fluid.

### Design of closed-circuit EFMs

EFMs are composed of one or more fiber pumps (Fig. 1A, i), connected at both ends to one or more thin McKibben actuators (Fig. 1A, ii and iii) that are sealed at their distal ends. We designed the muscles as a closed system without the need for an external reservoir, enabling untethered operation (Movie 1 and movie S11). Once the system is filled with dielectric liquid, the total liquid volume in the circuit (pump and actuators) does not change during operation. Each actuator acts as a reservoir for its antagonist, making EFMs compact and portable.

The system was activated by applying a voltage difference to the two electrical terminals of the fiber pump (Fig. 1C, i), which, drawing energy from the power supply, moves liquid from one actuator, causing it to extend, and transfers it to the other, which contracts [Fig. 1C (ii), Movie 1, and movie S1]. When initially filling the muscle with dielectric liquid, we added an excess liquid volume to pressurize the system at a bias pressure that we could regulate.

### Characterization of McKibben actuators, fiber pumps, and individual muscle pairs (one fiber pump connected to two McKibben actuators)

The experimental setup shown in Fig. 3A involved two McKibben actuators in an antagonistic configuration, driven by one fiber pump connected between them. The muscle was actuated using a compact high-voltage dc power supply (0 to 10 kV and 1.5 mA), and the pressure difference across the pump was measured via gauge sensors at the inlet and outlet. Displacement of each actuator under both symmetric and asymmetric loading conditions (100 to 500 g) was recorded using linear potentiometers. For fiber pump characterization, the flow rate was measured by integrating a flow meter in series with the pump (fig. S6A). All data—including pressure, displacement, flow rate, voltage, and current—were recorded using two synchronized DAQ (data acquisition) devices at 500 Hz. The circuit was filled with dielectric fluid and sealed before each test.

#### *Characterization of McKibben actuators*

We evaluated the displacement response of vertically mounted McKibben actuators ($n = 3$) under varying bias pressures and loads using a simplified version of the experimental setup, with a gauge pressure and linear displacement sensor. A syringe pump injected dielectric fluid at a controlled rate, and actuator deformation was recorded using the same DAQ device.

These actuators contract when pressurized. We characterized their contraction as a function of pressure and volume for actuators with an OD of 1.5 mm while lifting different loads. The resulting curves (Fig. 2A, ii and iii) show the characteristic pressure-contraction and volume-contraction responses of these actuators. Here, both pressure and volume are defined relative to the baseline values when the actuators are filled with liquid and undeformed. The pressure-contraction response curve initially shows a flat response, especially under high loads, before the response steepens at higher pressure values. This nonlinear behavior, typical of McKibben actuators (*59*), results in small contractions until the steep response region is reached. In the final part of the pressure range, the response tends to flatten again as maximum contraction is reached.

#### *Pressure-flow characterization of fiber pumps*

We characterized fiber pumps ($n = 3$) under varying pressure conditions (open/closed circuit, with and without bias pressure) using fresh dielectric liquid for each test. Pump flow rate and pressure were measured across voltage steps from 1 to 8 kV. The devices were tested under three configurations of fluidic circuit: constant atmospheric pressure (open circuit, in which the inlet of the pump is connected to a liquid reservoir open to the environment), closed circuit (no fluid reservoir) with no bias pressure applied ($p_{bias} = 0$ kPa), and closed circuit with excess liquid added until reaching a bias pressure $p_{bias} = 75$ kPa.

The results show that the pressure and flow rate increase more than linearly with voltage. Performance at the same voltage was independent of the fluidic circuit configuration. However, the closed-circuit configuration with no bias pressure ($p_{bias} = 0$ kPa) could be tested only up to 4 kV because of electrical breakdown triggered by cavitation of the dielectric liquid. Both the open circuit and the closed circuit with $p_{bias} = 75$ kPa could be tested until 7 kV and showed the same performance. The configuration with $p_{bias} = 75$ kPa could be safely tested up to 8 kV, showing good stability and producing a maximum pressure differential of 320 kPa (Fig. 2B, ii) and a maximum flow rate of 95 ml/min (Fig. 2B, iii).

### *Characterization of individual muscle pairs (one fiber pump connected to two McKibben actuators)*

Performance of muscle pairs was characterized under varying voltage, bias pressure, and load conditions. Muscle pair mass measurements are provided in table S2. Each test was performed on $n = 3$ devices, with five actuation cycles at 0.05 Hz per device. Before cyclic actuation, the applied voltage was held constant for 30 s to allow stabilization. Data points represent 10-s averages per cycle, further averaged across devices.

### *Dynamic characterization of individual muscle pairs*

The dynamic tests consisted of varying frequency from 0.25 to 10 Hz under a fixed condition of 75-kPa bias pressure at 7 kV. The power supply output was adjusted and allowed to stabilize for 30 s before initiating the cyclic tests, after which each frequency was applied for 20-s-long cycles per device, across three identical devices.

### *Characterization of robotic applications*

For all demonstrations in Figs. 4 to 6, we applied the driving signals using a compact custom 30-W power supply with an embedded dc converter (Advanced Energy, 10A24-P30-I5) shown in fig. S12. For the lever arm demo in Fig. 4, we analyzed jump heights and corresponding time stamps by recording motion with a high-speed camera (Sony Alpha 7 III) at a frame rate of 120 fps. For the bundle demo in Fig. 5, we measured displacements using linear potentiometers, and response time was captured using a dual DAQ (Digilent Discovery MCC-234) setup. For the woven demo in Fig. 6, response times and bending angles were determined by analyzing arm motion recorded with a Canon EOS 5D Mark IV camera using Kinovea (2023.1.2) analysis software.

### *Statistical analysis*

Muscle pair experiments were performed on $n = 3$ devices over 5 cycles per condition, unless otherwise noted in the figure captions. Each robotic demonstration was tested on a single device with 10 cycles per data point (mean ± SD). Data were processed in Python, and signals were downsampled to 50 Hz. Duty cycle periods were segmented using the electrical drive signal.

## Supplementary Materials

**The PDF file includes:**

Materials and Methods
Supplementary Methods
Figs. S1 to S15
Tables S1 to S3
Legends for movies S1 to S11
References (*60*–*69*)

**Other Supplementary Material for this manuscript includes the following:**

Movies S1 to S11

## REFERENCES AND NOTES


1. C. Laschi, B. Mazzolai, M. Cianchetti, Soft robotics: Technologies and systems pushing the boundaries of robot abilities. *Sci. Robot.* **1**, eaah3690 (2016).
2. V. Sanchez, C. J. Walsh, R. J. Wood, Textile technology for soft robotic and autonomous garments. *Adv. Funct. Mater.* **31**, 2008278 (2021).
3. K. Suzumori, S. Iikura, H. Tanaka, "Development of flexible microactuator and its applications to robotic mechanisms," in *Proceedings 1991 IEEE International Conference on Robotics and Automation* (IEEE, 1991), pp. 1622–1627.
4. F. Ilievski, A. D. Mazzeo, R. F. Shepherd, X. Chen, G. M. Whitesides, Soft robotics for chemists. *Angew. Chem. Int. Ed. Engl.* **50**, 1890–1895 (2011).
5. Z. Wang, K. Or, S. Hirai, A dual-mode soft gripper for food packaging. *Robot. Auton. Syst.* **125**, 103427 (2020).
6. K. C. Galloway, K. P. Becker, B. Phillips, J. Kirby, S. Licht, D. Tchernov, R. J. Wood, D. F. Gruber, Soft robotic grippers for biological sampling on deep reefs. *Soft Robot.* **3**, 23–33 (2016).
7. R. F. Shepherd, F. Ilievski, W. Choi, S. A. Morin, A. A. Stokes, A. D. Mazzeo, X. Chen, M. Wang, G. M. Whitesides, Multigait soft robot. *Proc. Natl. Acad. Sci. U.S.A.* **108**, 20400–20403 (2011).
8. D. Drotman, S. Jadhav, D. Sharp, C. Chan, M. T. Tolley, Electronics-free pneumatic circuits for controlling soft-legged robots. *Sci. Robot.* **6**, eaay2627 (2021).
9. K. Suzumori, S. Endo, T. Kanda, N. Kato, H. Suzuki, "A bending pneumatic rubber actuator realizing soft-bodied manta swimming robot," in *IEEE International Conference on Robotics and Automation (ICRA)* (IEEE, 2007), pp. 4975–4980.
10. C. A. Aubin, S. Choudhury, R. Jerch, L. A. Archer, J. H. Pikul, R. F. Shepherd, Electrolytic vascular systems for energy-dense robots. *Nature* **571**, 51–57 (2019).
11. G. Li, T.-W. Wong, B. Shih, C. Guo, L. Wang, J. Liu, T. Wang, X. Liu, J. Yan, B. Wu, F. Yu, Y. Chen, Y. Liang, Y. Xue, C. Wang, S. He, L. Wen, M. T. Tolley, A.-M. Zhang, C. Laschi, T. Li, Bioinspired soft robots for deep-sea exploration. *Nat. Commun.* **14**, 7097 (2023).
12. C. T. O'Neill, C. M. McCann, C. J. Hohimer, K. Bertoldi, C. J. Walsh, Unfolding textile-based pneumatic actuators for wearable applications. *Soft Robot.* **9**, 163–172 (2022).
13. Y. M. Zhou, C. J. Hohimer, H. T. Young, C. M. McCann, D. Pont-Esteban, U. S. Civici, Y. Jin, P. Murphy, D. Wagner, T. Cole, N. Phipps, H. Cho, F. Bertacchi, I. Pignataro, T. Proietti, C. J. Walsh, A portable inflatable soft wearable robot to assist the shoulder during industrial work. *Sci. Robot.* **9**, eadi2377 (2024).
14. M. Takeichi, K. Suzumori, G. Endo, H. Nabae, "Development of a 20-m-long Giacometti arm with balloon body based on kinematic model with air resistance," in *2017 IEEE/RSJ International Conference on Intelligent Robots and Systems (IROS)* (IEEE, 2017), pp. 2710–2716.
15. A. Poulin, S. Rosset, H. R. Shea, Printing low-voltage dielectric elastomer actuators. *Appl. Phys. Lett.* **107**, 244104 (2015).
16. F. B. Madsen, A. E. Daugaard, S. Hvilsted, A. L. Skov, The current state of silicone-based dielectric elastomer transducers. *Macromol. Rapid Commun.* **37**, 378–413 (2016).
17. M. Duduta, E. Hajiesmaili, H. Zhao, R. J. Wood, D. R. Clarke, Realizing the potential of dielectric elastomer artificial muscles. *Proc. Natl. Acad. Sci. U.S.A.* **116**, 2476–2481 (2019).
18. J. Shintake, V. Cacucciolo, H. Shea, D. Floreano, Soft biomimetic fish robot made of dielectric elastomer actuators. *Soft Robot.* **5**, 466–474 (2018).
19. S. Kim, Y.-H. Hsiao, Z. Ren, J. Huang, Y. Chen, Acrobatics at the insect scale: A durable, precise, and agile micro–aerial robot. *Sci. Robot.* **10**, eadp4256 (2025).
20. M. Taghavi, T. Helps, J. Rossiter, Electro-ribbon actuators and electro-origami robots. *Sci. Robot.* **3**, eaau9795 (2018).
21. E. Acome, S. K. Mitchell, T. G. Morrissey, M. B. Emmett, C. Benjamin, M. King, M. Radakovitz, C. Keplinger, Hydraulically amplified self-healing electrostatic actuators with muscle-like performance. *Science* **359**, 61–65 (2018).
22. E. Leroy, R. Hinchet, H. Shea, Multimode hydraulically amplified electrostatic actuators for wearable haptics. *Adv. Mater.* **32**, e2002564 (2020).
23. I. D. Sîrbu, G. Moretti, G. Bortolotti, M. Bolignari, S. Diré, L. Fambri, R. Vertechy, M. Fontana, Electrostatic bellow muscle actuators and energy harvesters that stack up. *Sci. Robot.* **6**, eaaz5796 (2021).
24. N. Kellaris, V. Gopaluni Venkata, G. M. Smith, S. K. Mitchell, C. Keplinger, Peano-HASEL actuators: Muscle-mimetic, electrohydraulic transducers that linearly contract on activation. *Sci. Robot.* **3**, eaar3276 (2018).
25. F. Hartmann, M. Baskaran, G. Raynaud, M. Benbedda, K. Mulleners, H. Shea, Highly agile flat swimming robot. *Sci. Robot.* **10**, eadr0721 (2025).
26. T. Helps, C. Romero, M. Taghavi, A. T. Conn, J. Rossiter, Liquid-amplified zipping actuators for micro-air vehicles with transmission-free flapping. *Sci. Robot.* **7**, eabi8189 (2022).
27. Z. Yoder, D. Macari, G. Kleinwaks, I. Schmidt, E. Acome, C. Keplinger, A soft, fast and versatile electrohydraulic gripper with capacitive object size detection. *Adv. Funct. Mater.* **33**, 2209080 (2023).
28. Z. Kang, L. Yu, Y. Nie, M. Skowyra, S. Zhang, A. L. Skov, Fiber-format dielectric elastomer actuators by the meter. *Adv. Funct. Mater.* **34**, 2314056 (2024).
29. Q. Shao, L. Zhou, J. Zhou, X. Liu, H. Zhao, Long, fibrous, and tailorable dielectric elastomer artificial muscles via mask-free stamping of carbon nanotube electrodes. *Adv. Funct. Mater.* **35**, 2570101 (2025).
30. S. Oh, R. Tabassian, P. Thangasamy, M. Mahato, V. H. Nguyen, S. Nam, Z. Huapeng, I.-K. Oh, Cooling-accelerated nanowire-nitinol hybrid muscle for versatile prosthetic hand and biomimetic retractable claw. *Adv. Funct. Mater.* **32**, 2111145 (2022).
31. M.-S. Kim, J.-K. Heo, H. Rodrigue, H.-T. Lee, S. Pané, M.-W. Han, S.-H. Ahn, Shape memory alloy (SMA) actuators: The role of material, form, and scaling effects. *Adv. Mater.* **35**, e2208517 (2023).
32. S. J. Park, K. Choi, H. Rodrigue, C. H. Park, Soft exosuit based on fabric muscle for upper limb assistance. *IEEE/ASME Trans. Mechatron.* **28**, 26–37 (2023).
33. H. Zhang, H. Shea, Clutchable fabric actuator for energy-efficient wearable robots. *Adv. Funct. Mater.* **35**, 2415099 (2025).
34. H. Yang, X. Yin, C. Zhang, B. Chen, P. Sun, Y. Xu, Weaving liquid crystal elastomer fiber actuators for multifunctional soft robotics. *Sci. Adv.* **11**, eads3058 (2025).
35. X. Hu, H. Li, J. Wang, X. Bao, K. Zhao, J. Di, Y. Liang, J. Ding, Multi-stimuli, large-stroke hybrid carbon fiber-based artificial muscles. *Macromol. Mater. Eng.* **309**, 2300252 (2024).

36. J. Qiao, J. Di, S. Zhou, K. Jin, S. Zeng, N. Li, S. Fang, Y. Song, M. Li, R. H. Baughman, Q. Li, Large-stroke electrochemical carbon nanotube/graphene hybrid yarn muscles. *Small* **14**, e1801883 (2018).
37. Z. Yoder, E. H. Rumley, I. Schmidt, P. Rothemund, C. Keplinger, Hexagonal electrohydraulic modules for rapidly reconfigurable high-speed robots. *Sci. Robot.* **9**, eadl3546 (2024).
38. M. Smith, V. Cacucciolo, H. Shea, Fiber pumps for wearable fluidic systems. *Science* **379**, 1327–1332 (2023).
39. S. Kurumaya, H. Nabae, G. Endo, K. Suzumori, Design of thin McKibben muscle and multifilament structure. *Sens. Actuators A: Phys.* **261**, 66–74 (2017).
40. A. Kodaira, H. Nabae, T. Horiuchi, K. Asaka, G. Endo, K. Suzumori, "Au/Pt double-layer electrodes and expanding internal chamber for improving air-hose-free thin McKibben muscles," in *2021 IEEE 4th International Conference on Soft Robotics (RoboSoft)* (IEEE, 2021), pp. 419–426.
41. X. Chen, W. Zhu, W. Liang, Y. Lang, Q. Ren, Control of antagonistic McKibben muscles via a bio-inspired approach. *J. Bionic. Eng.* **19**, 1771–1789 (2022).
42. Y. Yu, J. Wang, X. Han, S. Yang, G. An, C. Lu, Fiber-shaped soft actuators: Fabrication, actuation mechanism and application. *Adv. Fiber Mater.* **5**, 868–895 (2023).
43. S. Tanaka, H. Nabae, K. Suzumori, Back-stretchable McKibben muscles: Expanding the range of antagonistic muscle driven joints. *IEEE Robot. Autom. Lett.* **8**, 5331–5337 (2023).
44. 3M Novec 7100 engineered fluid; https://multimedia.3m.com/mws/media/199818O/3m-novec-7100-engineered-fluid.pdf.
45. Y. Peng, D. Li, X. Yang, Z. Ma, Z. Mao, A review on electrohydrodynamic (EHD) pump. *Micromachines* **14**, 321 (2023).
46. S. Wakimoto, K. Suzumori, J. Takeda, "Flexible artificial muscle by bundle of McKibben fiber actuators," in *2011 IEEE/ASME International Conference on Advanced Intelligent Mechatronics (AIM)* (IEEE, 2011), pp. 457–462.
47. S. Kurumaya, K. Suzumori, H. Nabae, S. Wakimoto, Musculoskeletal lower-limb robot driven by multifilament muscles. *Robomech J.* **3**, 18 (2016).
48. S. Seok, A. Wang, M. Y. Chuah, D. J. Hyun, J. Lee, D. M. Otten, J. H. Lang, S. Kim, Design principles for energy-efficient legged locomotion and implementation on the MIT Cheetah robot. *IEEE/ASME Trans. Mechatron.* **20**, 1117–1129 (2015).
49. B. Katz, J. D. Carlo, S. Kim, "Mini Cheetah: A platform for pushing the limits of dynamic quadruped control," in *2019 International Conference on Robotics and Automation (ICRA)* (IEEE, 2019), pp. 6295–6301.
50. S. Pourazadi, A. Shagerdmootaab, H. Chan, M. Moallem, C. Menon, On the electrical safety of dielectric elastomer actuators in proximity to the human body. *Smart Mater. Struct.* **26**, 115007 (2017).
51. M. Hassani Sadi, Z. Sadeghi, J. Bauman, A comprehensive review of universal fast-charging techniques for 400-V and 800-V electric vehicles. *IEEE Access* **13**, 153212–153233 (2025).
52. Y. Luo, J.-B. Chossat, M. Schouten, H. Shea, "Increasing the performance of EHD fiber pumps by scaling and by changing to a more sustainable working fluid," presentation at the 2024 MRS Fall Meeting & Exhibit (Materials Research Society, 2024); https://mrs.org/meetings-events/annual-meetings/archive/meeting/presentations/view/2024-fall-meeting/2024-fall-meeting-4151248.
53. C. Zhang, Y. Duan, Z. Jiao, Y. Zhu, B. Xu, H. Yang, J. Zhang, Functional fluid-based soft robotic actuation. *Adv. Mater.* **37**, e2502669 (2025).
54. S. Yokota, Micro actuators by making use of jet flows due to electro-conjugate fluid. *Mech. Based Des. Struct. Mach.* **36**, 330–345 (2008).
55. K. Shimizu, K. Murakami, N. Ogawa, H. Akai, J. Shintake, Polyvinyl chloride-added dibutyl adipate for high-performance electrohydrodynamic pumps. *Front. Robot. AI* **10**, 1109563 (2023).
56. S. Yokota, Y. Otsubo, K. Edamura, Electro-sensitive movable fluids, methods of using the same and motors for the electro-sensitive movable fluids, US Patent US6030544A (2000); https://patents.google.com/patent/US6030544A/en.
57. R. Kanno, K. Shimizu, K. Murakami, Y. Shibahara, N. Ogawa, H. Akai, J. Shintake, Silicone-based highly stretchable multifunctional fiber pumps. *Sci. Rep.* **14**, 4618 (2024).
58. T. Morita, T. Kurosawa, K. Aoyama, H. Kaimoto, Y. Kuwajima, S. Maeda, Y. Kakehi, "Design and rapid fabrication of integrated fiber-based EHD pumps," in *Proceedings of the Extended Abstracts of the CHI Conference on Human Factors in Computing Systems* (Association for Computing Machinery, 2025), pp. 1–5.
59. C.-P. Chou, B. Hannaford, Measurement and modeling of McKibben pneumatic artificial muscles. *IEEE Trans. Robot. Autom.* **12**, 90–102 (1996).
60. M. K. Russel, P. R. Selvaganapathy, C. Y. Ching, Electrohydrodynamic injection micropump with composite gold and single-walled carbon nanotube electrodes. *J. Microelectromech. Syst.* **24**, 1557–1564 (2015).
61. H. Yu, J. Yu, C. Ma, Design, fabrication and experimental research for an electrohydrodynamic micropump. *Sci. China Technol. Sci.* **53**, 2839–2845 (2010).
62. R. W. Ogden, "Elements of the theory of finite elasticity," in *Nonlinear Elasticity: Theory and Applications*, R. W. Ogden, Y. B. Fu, Eds., *London Mathematical Society Lecture Note Series* (Cambridge Univ. Press, 2001), pp. 1–57.
63. C. O. Horgan, J. G. Murphy, Magic angles for fibrous incompressible elastic materials. *Proc. A* **474**, 20170728 (2018).
64. B. Tondu, Modelling of the McKibben artificial muscle: A review. *J. Intell. Mater. Syst. Struct.* **23**, 225–253 (2012).
65. R. H. Gaylord, Fluid actuated motor system and stroking device, US Patent US2844126A (1958); https://patents.google.com/patent/US2844126A/en.
66. H. F. Schulte, "The characteristics of the McKibben artificial muscle" in *The Application of External Power in Prosthetics and Orthotics* (National Academy of Sciences–National Research Council, 1961), pp. 94–115.
67. A. N. Gent, On the relation between indentation hardness and Young's modulus. *Rubber Chem. Technol.* **31**, 896–906 (1958).
68. P. Rothemund, N. Kellaris, S. K. Mitchell, E. Acome, C. Keplinger, HASEL artificial muscles for a new generation of lifelike robots—Recent progress and future opportunities. *Adv. Mater.* **33**, e2003375 (2021).
69. A. Maziz, A. Concas, A. Khaldi, J. Stålhand, N.-K. Persson, E. W. H. Jager, Knitting and weaving artificial muscles. *Sci. Adv.* **3**, e1600327 (2017).


**Acknowledgments:** We thank M. Smith and H. Shea of EPFL-LMTS (École Polytechnique Fédérale de Lausanne–Soft Transducers Lab) for help with the fiber pump manufacturing process and the insightful discussions on electrofluidic artificial muscles. We thank F. Gargano of Omnigrasp SRL for assembling the high-voltage power supply and providing support. We also thank S. Seiki (Japan), C. Bensahel, S. Nicita, and R. Didero for support with textile integration methods. We thank H. Shea, C. Laschi, and D. Floreano for providing helpful feedback on the manuscript. **Funding:** This project was cofunded by the European Union [European Research Council (ERC), ROBOFLUID, 101116856]. Views and opinions expressed are, however, those of the authors only and do not necessarily reflect those of the European Union or the ERC. Neither the European Union nor the granting authority can be held responsible for them. The project has received funding from the Massachusetts Institute of Technology Media Laboratory Multi-Sponsored Consortium. **Author contributions:** Conceptualization: O.K.A. and V.C. Methodology: O.K.A., G.V., and V.C. Investigation: O.K.A., G.P., W.B., G.V., and V.C. Visualization: O.K.A., G.P., and G.V. Funding acquisition: O.K.A., H.I., and V.C. Project administration: H.I. and V.C. Supervision: V.C. Writing—original draft: O.K.A., G.P., G.V., and V.C. Writing—review and editing: O.K.A., G.P., W.B., G.V., H.I., and V.C. **Competing interests:** The authors declare that they have no competing interests. **Data, code, and materials availability:** All data needed to support the conclusions of this manuscript are included in the main text, Supplementary Materials, and in the Zenodo repository: https://doi.org/10.5281/zenodo.18678491. All reagents and materials associated with this study are listed in Materials and Methods and/or are available commercially.

Submitted 29 May 2025
Accepted 25 February 2026
Published 25 March 2026
10.1126/scirobotics.ady6438

Science Robotics

# Electrofluidic fiber muscles

O. K. Afsar, G. Pupillo, G. Vitucci, W. Babatain, H. Ishii, and V. Cacucciolo

*Sci. Robot.* **11** (112), eady6438. DOI: 10.1126/scirobotics.ady6438







*Science Robotics* (ISSN 2470-9476) is published by the American Association for the Advancement of Science. 1200 New York Avenue NW, Washington, DC 20005. The title *Science Robotics* is a registered trademark of AAAS.